Photochemical & Photobiological Sciences (2023) 22:1655–1671
https://doi.org/10.1007/s43630-023-00401-9

ORIGINAL PAPERS

5-Deazaalloxazine as photosensitizer of singlet oxygen and potential redox-sensitive agent

Małgorzata Insińska-Rak[1] · Anna Golczak[1] · Mateusz Gierszewski[2] · Zubair Anwar[1] · Volodymyr Cherkas[3] · Dorota Kwiatek[3] · Ewa Sikorska[4] · Igor Khmelinskii[5] · Gotard Burdziński[2] · Radek Cibulka[6] · Lucyna Mrówczyńska[7] · Jacek Lukasz Kolanowski[3] · Marek Sikorski[1]

Received: 7 October 2022 / Accepted: 28 February 2023 / Published online: 19 March 2023

Abstract

Flavins are a unique class of compounds that combine the features of singlet oxygen generators and redox-dependent fluorophores. From a broad family of flavin derivatives, deazaalloxazines are significantly underdeveloped from the point of view of photophysical properties. Herein, we report photophysics of 5-deazaalloxazine (**1a**) in water, acetonitrile, and some other solvents. In particular, triplet excited states of **1a** in water and in acetonitrile were investigated using ultraviolet–visible (UV–Vis) transient absorption spectroscopy. The measured triplet lifetimes for **1a** were all on the microsecond time scale (≈ 60 µs) in deoxygenated solutions. The quantum yield of $S_1 \rightarrow T_1$ intersystem crossing for **1a** in water was 0.43 based on T_1 energy transfer from **1a** to indicaxanthin (**5**) acting as acceptor and on comparative actinometric measurements using benzophenone (**6**). **1a** was an efficient photosensitizer for singlet oxygen in aerated solutions, with quantum yields of singlet oxygen in methanol of about 0.76, compared to acetonitrile ~ 0.74, dichloromethane ~ 0.64 and 1,2-dichloroethane ~ 0.54. Significantly lower singlet oxygen quantum yields were obtained in water and deuterated water (Φ_Δ ~ 0.42 and 0.44, respectively). Human red blood cells (RBC) were used as a cell model to study the antioxidant capacity in vitro and cytotoxic activity of **1a**. Fluorescence-lifetime imaging microscopy (FLIM) data were analyzed by fluorescence lifetime parameters and distribution for different parts of the emission spectrum. Comparison of multidimensional fluorescent properties of RBC under physiological-like and oxidative-stress conditions in the presence and absence of **1a** suggests its dual activity as probe and singlet-oxygen generator and opens up a pathway for using FLIM to analyze complex intracellular behavior of flavin-like compounds. These new data on structure–property relationship contribute to the body of information required for a rational design of flavin-based tools for future biological and biochemical applications.

Graphical abstract

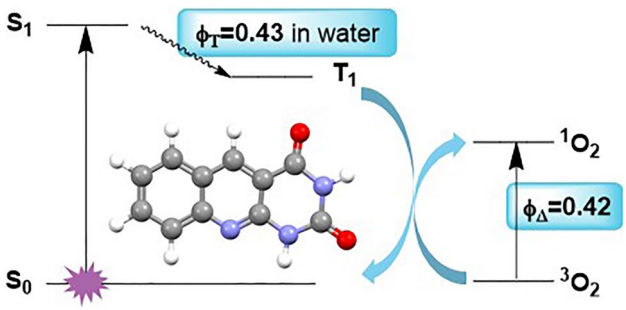

Keywords 5-deazaflavin · 5-deazaalloxazine · Alloxazine · Singlet oxygen · Triplet excited state · Red blood cells · Oxidative stress · Fluorescence-lifetime imaging microscopy (FLIM)

Extended author information available on the last page of the article

1 Introduction

From a broad family of flavin derivatives, flavins (isoalloxazines), 5-deazaflavins (deazaisoalloxazines) and structurally related alloxazines have become attractive candidates for photochemical and biological studies. Flavins combine the features of photooxygenation via type I and/or type II mechanism being also a pH and redox-dependent fluorophores [1–4] and an increasing body of structure–property relationship information, which makes flavins well poised for fine tuning of their properties at will. We are undertaking this study to understand the relationship between the structure and singlet-oxygen generation and fluorescence properties to build up a necessary background information for rational design of tools based on flavins for biological and biochemical applications in the future. On the other hand, despite the fact that 5-deazaalloxazines have already been prepared and studied, their photophysical properties are still significantly underdeveloped.

Isoalloxazines and alloxazines and their deaza derivatives differ by only the methine group versus nitrogen in position 5 (see Fig. 1, for the structural difference between 5-deazaalloxazine **1a** and alloxazine **2a**). Note that this structural feature brings many positive properties in isoalloxazine series and applications in photoredox catalysis. For example, deazaisoalloxazines have higher triplet excited state energies compared to isoalloxazines, which is their advantage in reactions occurring via energy transfer [5]. Deazaisoalloxazines have also more negative reduction potential in comparison to isoalloxazines, and therefore they are more suitable for reductive photocatalysis [6]. Moreover, deazaisoalloxazines have higher photostability. One can expect a similar trend comparing alloxazines to deazaalloxazines.

Along with characterizing the singlet excited states, a description of triplet excited states is also important for understanding the molecular photophysical properties. Generally, triplet excited states are involved in the generation of reactive oxygen species, including singlet oxygen, and therefore in photooxidation reactions [7–14]. Transient UV–Vis absorption spectra have been recorded upon pulsed laser excitation of various alloxazine derivatives in organic and aqueous solutions [15–20]. Triplet excited states have their lifetimes in the microsecond time range, as the T_1—S_0 transition is spin-prohibited. Theoretical calculations have predicted that the lowest-energy triplet → triplet (T-T) electronic transitions to be of π, π* character in these compounds [9, 21, 22].

The triplet excited states of various alloxazine derivatives, including those of lumichrome (**2b**) and its derivatives, have been explored in aqueous solutions [20, 23]. In particular, two different species have been detected for lumichrome and 1-methyllumichrome in deoxygenated aqueous solutions at pH ≈ 6 [20, 24]. One of these had a relatively broad absorption band at about 550 nm and 20 μs

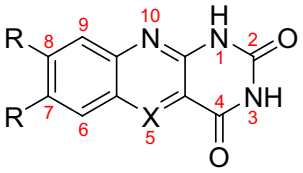

cmpd	X	R
1a	CH	H
2a	N	H
2b	N	Me

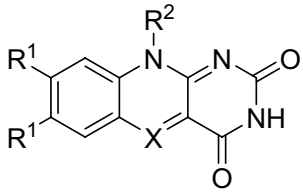

cmpd	X	R^1	R^2
3a	CH	H	Et
3b	CH	Me	ribityl
4a	N	Me	Me
4b	N	Me	ribityl

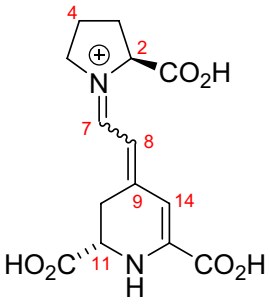

5

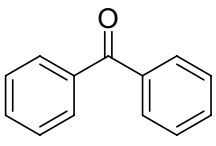

6

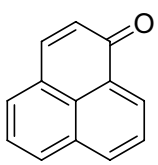

7

Fig. 1 Structures of 5-deazaalloxazine (**1a**), alloxazine (**2a**), lumichrome (**2b**), 10-ethyl-5-deazaisoalloxazine (**3a**), 5-deazariboflavin (**3b**), lumiflavin (**4a**), riboflavin (**4b**), indicaxanthin (**5**), benzophenone (**6**), and perinaphthenone (**7**)

decay time constant, while the other had a weaker absorption band at about 450 nm and 400 µs decay time. The short-lived species has been identified as the triplet state of the neutral form of lumichrome and 1-methyllumichrome, whereas the long-lived species was the radical anion form of the parent molecule [25, 26]. Note also that the triplet excited state of the lumichrome in oxygen-free solutions was quenched by its ground-state molecules in the concentration range from 1×10^{-5} M to 6×10^{-5} M and higher. The intersystem crossing yields in lumichrome and 1-methyllumichrome were quite high, 0.69 and 0.50, respectively [20]. The presence of the methyl group substituent had little effect on the triplet lifetime 17 µs for lumichrome vs. 18 µs for 1-methyllumichrome in deoxygenated aqueous solutions at pH ≈ 6 [20].

Some flavin derivatives, such as iso- and alloxazines, function as efficient photosensitizers of singlet oxygen [8, 27, 28]. In general, alloxazines were better photosensitizers of singlet oxygen than isoalloxazines. For example, lumichrome (**2b**, an alloxazine) produced singlet oxygen with the quantum yield $\Phi_\Delta = 0.85$, while lumiflavin (**4a**, an isoalloxazine) had $\Phi_\Delta = 0.48$ (both values reported in methanol, with similar trends obtained in other solvents) [27]. Note that 5-deazariboflavin (**3b**) was also an efficient photosensitizer of singlet oxygen, although its Φ_Δ was lower than that of riboflavin (**4b**) under the same conditions. Namely, Φ_Δ values for **3b** and **4b** were 0.33 and 0.51, respectively, in methanol [9, 16]. However, there is still a lack of information on the singlet oxygen production by deazaalloxazines like **1a** and its derivatives.

In the present work, the properties of **1a** in its triplet excited state were explored. Transient UV–Vis absorption spectra were recorded in water (pH ~ 6) and acetonitrile. The quantum yield of intersystem crossing (Φ_{ISC}) was also determined for **1a** in aqueous solutions. Finally, singlet oxygen production sensitized by **1a** was explored in organic solvents, water, and deuterated water.

In order to demonstrate potential applications of **1a** in biological systems, its cytotoxicity (biocompatibility) was evaluated in vitro using human red blood cells (RBC). Hemolysis is the most commonly employed toxicity assessment method [29] and human RBC are used as model cells in biocompatibility studies of chemical compounds with potential biomedical applications [30]. In vivo, RBC are continuously exposed to reactive oxygen species (ROS) in the circulatory system, due to their role as oxygen transporters and to their frequent exposure to different xenobiotics [31]. Therefore, RBC are also an excellent model for the evaluation of the effects of ROS generated from *tert*-butyl hydroperoxide (**TB**) in the presence of compounds with potential antioxidant capacity.

2 Experimental

2.1 Materials

1a was synthesized in our group; see ref. [32] for the details of its synthesis and characteristics. Indicaxanthin (**5**) was used to determine the quantum yield of intersystem crossing for **1a** in aqueous solutions; the photophysics of **5** has been recently reported [33]. Benzophenone (**6**), perinaphthenone (**7**) and spectroscopic or HPLC-grade solvents (acetonitrile, methanol, dichloromethane, 1,2-dichloroethane and deuterated water) were all purchased from Sigma Aldrich.

The compounds studied were checked for purity and analyzed using TLC, ^{1}H NMR, ^{13}C NMR, HRMS, HPLC, spectral emission excitation matrix, absorption and fluorescence excitation spectra and elemental analysis.

5-Deazaalloxazine, pyrimido[4,5-b]quinoline-2,4(1H,3H)-dione, (**1a**) (m.p. > 350 °C with decomp, lit. m.p. > 320 °C [34]); ^{1}H NMR (DMSO-d_6): δ ppm: 7.55 (m, 1H, H-7); 7.85 (m, 2H, H-8 and H-9); 8.16 (m, 1H, H-6); 9.03 (s, 1H, H-C5); 11.62 (bs, 2H, N(1)-H and N(3)-H). (Atom numbering is shown in Fig. 1). ^{1}H NMR (TFA-d): δ ppm: 8.24 (t, 1H, H-7); 8.22 (d, 1H, H-9); 8.39 (m, 2H, H-8 and H-6); 9.78 (s, 1H, H-C5); ^{13}C NMR (DMSO-d_6): 111.6, 125.2, 125.7, 127.3, 130.4, 133.7, 139.6, 150.0, 150.7, 151.2, 162.8; Anal. Calculated for $C_{11}H_7N_3O_2$:C, 61.97; H, 3.31; N, 19.72. Found: C, 61.68; H, 3.20; N, 19.69; HRMS (ESI+) calculated for $C_{11}H_7N_3O_2Na$ ($[M+Na]^+$): 236.04305, found 236.04310; calculated for $C_{11}H_8N_3O_2$ ($[M+H]^+$): 214.06110, found 214.06104.

^{1}H NMR spectrum for **1a** was recorded in DMSO-d_6 and in TFA-d. The ^{1}H NMR spectra were recorded on a Varian Gemini 300 (300 MHz) Spectrometer. ^{13}C NMR spectra were recorded on a JNM-ECZL400S spectrometer (JEOL Ltd., 100.58 MHz for ^{13}C). High-resolution mass spectra were obtained on LTQ Orbitrap Velos (Thermo Scientific), equipped with a linear ion trap and orbitrap analyzer and on Agilent 7200B GC Q-TOF (Agilent Technologies) equipped with a quadrupole and time-of-flight (TOF) analyzer. The internal standard was TMS. ^{1}H NMR spectra of compounds studied were analyzed by comparison to those of similar compounds [34, 35] and by comparison to spectra calculated using the ACD/HNMR predictor.

Purity of the **1a** was further confirmed using HPLC analysis (see Fig. 12S) and by emission excitation matrix collected with the A-TEEMs™ (absorbance-transmission and fluorescence excitation-emission matrix), excitation spectra, and synchronous spectra. The EEM data (Fig. 2) indicate that the samples are pure at the spectroscopic and/or fluorescence grade level, according to the detection level of the system used. The purity of the system was also confirmed by the comparison of absorption and fluorescence excitation

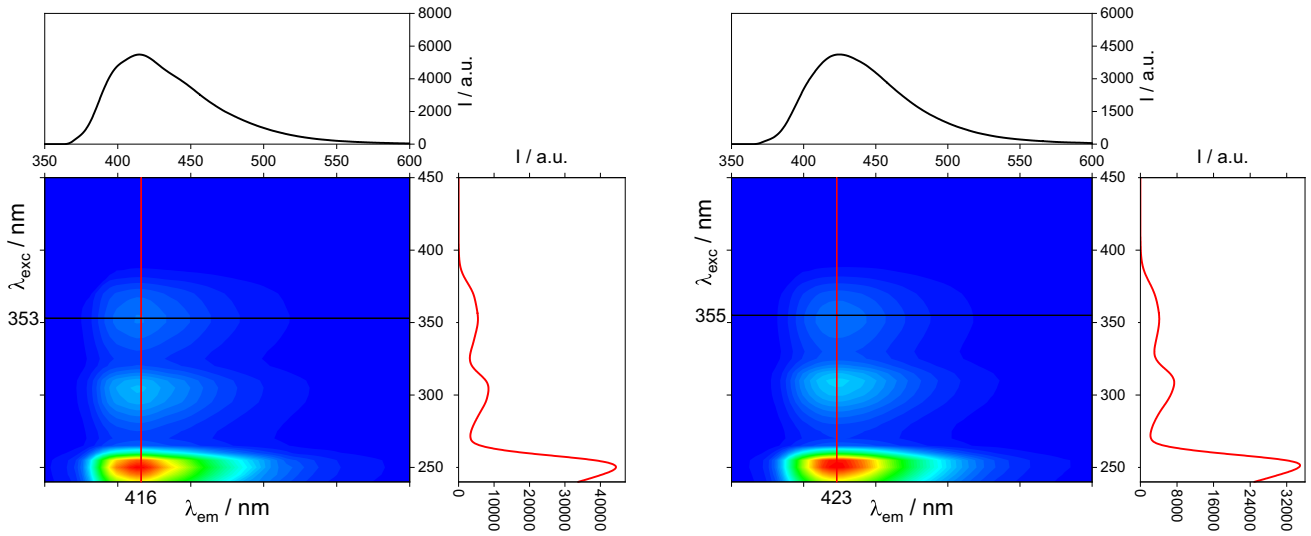

Fig. 2 Fully corrected Emission Excitation Matrix received with the A-TEEMs™ (absorbance-transmission and fluorescence excitation-emission matrix) method for **1a** in acetonitrile (left panel) and in water (right panel). The panels on top and on the right side of each EEM represent emission and fluorescence excitation spectra for selected wavelength of excitation and emission, respectively

spectra (Fig. 1SB). The purity was further confirmed by the synchronous scan spectrum, which showed only one maximum overlapping with the edge of the emission spectrum (Fig. 1SB). The data in Fig. 8S also supports the purity, as it shows no differences in the lifetimes recorded at different wavelengths of emission.

2.2 Absorption and emission measurements

UV–Vis absorption spectra were recorded on a Shimadzu UV-2550 spectrophotometer. Emission Excitation Matrix was collected with the A-TEEMs™ (absorbance-transmission and fluorescence excitation-emission matrix) method using a Horiba Scientific Aqualog spectrophotometer. Aqualog integrates its data acquisition functions directly with the Origin software. All EEMs data were corrected for the influence of inner filter effects (IFE) and Rayleigh masking. The measurements in water were performed under unbuffered conditions. However, detailed studies on **1a** as a function of pH have been presented in a separate paper, see [36]. The biological part has been conducted using PBS buffer. For general concern we also measured emission spectrum of **1a** in water with PBS, using for excitation 405 laser, the same as for FLIM experiments. The results, in particular fluorescence spectrum, were consistent with the experiments in unbuffered water.

2.3 Laser flash photolysis

Transient absorption spectra of **1a** in water (pH ~ 6) and acetonitrile were recorded using a nanosecond transient absorption spectrometer, described previously in detail [37], with 0.5 mJ excitation pulses ($\lambda_{exc} = 355$ nm) to the sample. Transient decays were recorded at individual wavelengths in 10 nm steps from 300 to 700 nm. The **1a** solutions in water and acetonitrile were deoxygenated by bubbling argon for 15 min prior to measurements. The experiments were carried out in square (1 cm × 1 cm) fused-silica cells. The same transient absorption spectrometer and procedures were used to record transient absorption spectra of **1a** and **5** mixtures, for the intersystem crossing yield measurements.

2.4 Singlet oxygen generation measurements

Characteristic steady-state emission spectra of singlet oxygen were recorded on a Jobin Yvon-Spex Fluorolog 3–221 spectrofluorometer with an H10330B-75 NIR-PMT module, sensitive in the 950–1700 nm NIR range. A xenon lamp with a monochromator was used as an excitation source for the steady-state emission spectra. Phosphorescence decays of $^1O_2$ decays were with a pulsed SpectraLED diode ($\lambda_{exc} = 371$ nm) at $\lambda_{em} = 1270$ nm on the same spectrofluorometer. The control experiments, showed that deoxygenation by argon bubbling produced no observable spectra or kinetics.

2.5 Determination of quantum yields of singlet oxygen production (Φ_Δ)

Quantum yields of singlet oxygen (Φ_Δ) generated in the presence of **1a** in organic solvents (acetonitrile, dichloromethane, and methanol), water and deuterated water were calculated using the results of steady-state measurements. Perinaphthenone (**7**) in the same solvents was used as a

reference, as it has $\Phi_{\Delta} = \Phi_{ST} = 0.95 \pm 0.05$, independent of the solvent used [38].

Initially, two sets of solutions were prepared as a series of dilutions with optical density maxima in the 0.02 to 0.10 range. These solutions were excited at their respective absorption maxima, containing (i) **1a** and (ii) **7** in the same solvent. Then, the characteristic emission spectra of singlet oxygen were recorded for **1a** and **7**, with the total area under the emission spectrum calculated separately for each of the substances. Finally, Φ_{Δ} was calculated according to Eq. (1):

$$\Phi_{1a} = \Phi_7 \frac{\mathrm{Grad}_{1a}}{\mathrm{Grad}_7} \quad (1)$$

Here, Φ_{1a} is the quantum yield of singlet oxygen production by **1a**; Φ_7 is the same for the reference sample (**7**); Grad_{1a} and Grad_7 are the slopes of the plots of integrated singlet oxygen intensity versus optical density of **1a** and **7**, respectively.

3 Hemocompatibility studies of 1a

3.1 Reagents

All reagents were purchased from Avantor Performance Materials Poland SA (Gliwice, Poland). Standard oxidant *tert*-butyl hydroperoxide (**TB**) was purchased from Sigma-Aldrich Chemie.

3.2 Human red blood cells

Fresh human red blood cells (RBC) suspensions as concentrates (hematocrit = 65%) were purchased from the blood bank in Poznań, according to the bilateral agreement no. ZP/907/1002/18 between the Blood Bank and Adam Mickiewicz University in Poznań. The RBC suspension was washed three times (3000 rpm, 10 min, + 4 °C) in 7.4 pH buffered phosphate saline (PBS – 137 mM NaCl, 2.7 mM KCl, 10 mM Na_2HPO_4, 1.76 mM KH_2PO_4) supplemented with 10 mM glucose. After washing, RBC were suspended in PBS buffer supplemented with 10 mM glucose at 1.65×10^9 cells/mL (hematocrit = 15%), stored at + 4 °C and used within 5 h.

3.3 In vitro hemolytic activity assay

The hemolytic potency of **1a** was determined by a standard hemolytic assay [39]. Briefly, RBC (1.65×10^8 cells/ml, hematocrit = 1.5%) were incubated in PBS buffer (7.4 pH) supplemented with 10 mM glucose and containing **1a** at a concentration equal to 1.0 mg/mL for 1 h and for 24 h at 37 °C in a thermoshaker (BioSan Thermo-Shaker TS-100 C, Biosan, Riga, Latvia). For the positive and negative controls, the RBC were incubated in deionized ice-cold water or in PBS buffer, respectively. Each sample was tested in triplicate and the experiments were repeated with RBC obtained from different blood donors. After incubation, the suspensions RBC were washed (3000 rpm, 10 min, 4 °C) (Sigma 3–30 K Sartorious AG, Gottingen, Germany) and the degree of hemolysis was estimated by measuring the absorbance values (Ab) of the sample supernatant at $\lambda = 540$ nm in an EPOLL2000 ECO spectrophotometer (PZ EMCO, Warsaw, Poland). The results were expressed as the percentage (%) of hemolysis, which was determined using the following equation:

$$\text{hemolysis}\,(\%) = \frac{\text{sample Ab}}{\text{positive control Ab}} \times 100 \quad (2)$$

where the positive control is Ab of supernatant obtained after incubation of RBC in ice-cold H_2O.

The results are presented as the mean values (n = 3) ± standard deviation (SD).

3.4 Fluorescence-lifetime imaging microscopy (FLIM) analysis of RBC

The RBC (1.65×10^8 cells/mL, hematocrit = 1.5%) were incubated in PBS buffer (7.4 pH) supplemented with 10 mM glucose and containing **1a** at the final concentration of 1.0 mg/mL for 1 h and for 24 h at 37 °C in a thermoshaker (BioSan Thermo-Shaker TS-100 C, Biosan, Riga, Latvia). To generate oxidative stress conditions within the RBC, cells were incubated with 250 µM *tert*-butyl hydroperoxide (**TB**), as the standard inducer of free radicals, for 1.5 h at 37 °C with gentle shaking. Each sample tube was tested in triplicate and the experiments were repeated four times with RBC obtained from different blood donors. After incubation, all RBC suspensions were washed (3000 rpm, 10 min, 4 °C), (Sigma 3–30 K Sartorious AG, Gottingen, Germany). The RBC suspensions (30 µL) were placed on microscope slides and covered with cover slips. A large number of intact RBC were studied in several separate experimental samples using a Abberior combined MINFLUX/STED superresolution laser scanning confocal microscopy system (Abberior Instruments, Germany) equipped with pulsed lasers, 6 high-sensitivity avalanche photodiode (APD) detectors in spectral configuration and dual channel time correlated single photon counting (TCSPC) system (PicoQuant, Germany). The microscope chassis was Olympus IX83 (Olympus, Japan). To avoid unnecessary image aberrations from refractive index mismatch water immersion objective Olympus 60 × NA 1.2 UPLSAPO60XW (Olympus, Japan) was used with optimized coverslip thickness correction collar. Two independent spectral detection channels were used to acquire

lifetime information simultaneously. The IRF FWHM was about 200 ps (for complete instrument), the modulation frequency was set to 80 MHz. TCSPC parameters were the following: 25 ns detection range, 1000 bins. Spectral settings for channels were selected based on fluorescent emission spectra acquired at the same microscope with all settings identical, except emission channel). FLIM was applied to study of **1a** as a possible redox-sensitive fluorescent probe in intact RBC under normal physiological (PBS buffer, 37 °C) and oxidative stress conditions (250 µM TB in PBS, 37 °C).

The following abbreviations for the differently treated samples will be used from now on:

RBC – control RBC (in PBS buffer),

RBC + TB – RBC incubated with 250 µM TB in PBS (1.5 h, 37 °C),

RBC + 1a – RBC incubated with 1.0 mg/mL **1a** (24 h, 37 °C) in PBS buffer,

RBC + 1a + TB – RBC preincubated with 1.0 mg/mL **1a** (24 h, 37 °C) in PBS buffer and then incubated with 250 µM TB (1.5 h, 37 °C).

The results and fluorescence lifetime distribution histograms were treated in SymPhoTime64 software (PicoQuant, Germany). IRF (instrument response function) was subtracted before the data fitting.

4 Results and discussion

In order to fully appreciate the implications of our data, it is instructive to place the photophysics of **1a** into a wider context. Therefore, the spectroscopic and photophysical properties of **1a** in various organic solvents and water are included in Table 1, together with the comparison data of alloxazine itself (**2a**), based on ref. [28], lumichrome (**2b**), based on ref. [27], and 10-ethyl-5-deazaisoalloxazine (**3a**), 5-deazariboflavin (**3b**), lumiflavin (**4a**), riboflavin (**4b**), data based, respectively, on ref. [40]. As this comparison illustrates, that while these isoalloxazines, alloxazines, and their deaza analogs share many structural features, they exhibit divergent spectral and photophysical properties. The difference between the alloxazinic and isoalloxazinic types of structures of molecules lies in the position of their central double bonds. Molecules with the alloxazinic structure have *s-cis*, whereas molecules with isoalloxazinic structure have an *s-trans* double-bond configuration. The structurally similar deaza derivatives, where the N-5 of the flavin iso- or alloxazine moiety is replaced by a methine group, are another common way of flavin modifications. These structural changes are mostly responsible for spectral and chemical differences. The longer-wavelength absorption bands (λ_1) are particularly sensitive to structural variation (see Fig. 1S). For example, isoalloxazines **4a** and **4b**, the deazaflavins **3a** and **3b**, and even alloxazine itself (**2a**) absorb in the range of 372–443 nm, allowing for convenient visible-light sources for excitation, while the unsubstituted deazaalloxazine **1a** absorbs only in the UV region. Shorter-wavelength absorption bands (λ_2) follow the same trend, although with a smaller range of variation.

Fluorescence parameters also follow some notable trends. The emission maxima (λ_F) values for the isoalloxazines (**4a** and **4b**) lie at the longest wavelengths (533 and 517 nm, respectively), while the 5-deaza analogues (**3a** and **3b**) exhibit a hypsochromic shift of 50–60 nm in emission. The lowest wavelength fluorescence emission maxima are from alloxazines (**2a** and **1a**), both of which emit below 435 nm. In terms of fluorescence quantum yields and lifetimes, derivatives **3b, 4a, 4b** and **1a** have a range of quantum yields (λ_F) from 0.11 to 0.24, with roughly the same fluorescence lifetimes (~4 ns), but shorter compared to lumiflavin (**4a**), whose fluorescence lifetime is almost double that value (7.7 ns). In contrast, the fluorescence quantum yield of unsubstituted alloxazine (**2a**) is two orders of magnitude lower (0.009), and its fluorescence lifetime is an order of magnitude lower (0.35 ns).

Figure 2 shows emission excitation matrix for **1a** in acetonitrile and in water. Measurements were made on an Aqualog from HORIBA with the ability to simultaneously acquire absorbance, transmittance, and fluorescence of a sample using a technique which combines A-TEEM spectroscopy with simultaneous multichannel CCD detection to provide extremely fast results. The EEMs collected by the instrument were corrected for the inner filter effect. The right-hand side of each EEM matrix shows the fluorescence excitation spectrum, and the top shows the corresponding emission spectrum. The excitation spectrum in each case is virtually the same as the corresponding absorption spectrum for **1a** in acetonitrile or in water at pH ~ 6.

According to theoretical calculations of singlet → singlet electronic transitions in alloxazine derivatives, each of the two lowest-energy π,π* transitions is accompanied by a closely-located weak n,π* transition, with the π,π* and n,π* transitions being isoenergetic in some cases [21, 41–45]. On the contrary, the corresponding 5-deaza derivatives (of which **1a** is the simplest representative) have the lowest-energy transition of π,π* character, and no accompanying n,π* transition, independent of the substitution pattern, see Fig. 11S [46, 47]. In fact, this feature is one of the most fundamental differences in electronic structure between alloxazines and their 5-deaza counterparts.

To explore the solvent effects, we investigated photophysical properties of **1a** in five solvents of different polarity, including protic and aprotic types. The results presented in Table 1 and presented earlier in [46] indicate the importance of intermolecular solute–solvent hydrogen bonding interactions in these compounds. As reported in Ref. [47] the Catalán and Kamlet–Taft parameters show a strong influence

Table 1 Spectroscopic and photophysical data for 5-deazaalloxazine (**1a**), in various organic solvents and water and alloxazine (**2a**), 10-ethyl-5-deazaisoalloxazine (**3a**), 5-deazariboflavin (**3b**), lumiflavin (**4a**) and riboflavin (**4b**) in acetonitrile

Compound	Solvent	λ_1/nm	λ_2/nm	λ_F/nm	Φ_F	τ_F/ns	$k_r/10^{-8}$ s^{-1}	$\Sigma k_{nr}/10^{-8}$ s^{-1}	τ_T/μs	Φ_Δ	$k_T^{[O_2]}/10^{-9}$ M^{-1} s^{-1}	[O_2]/mM	P_T^Δ
5-Deazaalloxazine (**1a**)	Acetonitrile	351[a]	296[a]	405[a]	0.18[a]	3.6[a]	0.50[a]	2.28	61	0.74	1.2	2.42[b]	0.99
	Methanol	353[a]	307[a]	416[a]	0.24[a]	5.1[a]	0.47	1.49	13	0.76	1.3	2.15[b]	0.97
	Dichloromethane	352[a]	309[a]	402[a]	0.03[a]	2.8[a]	0.11	3.46	21	0.64	1.3	0.71[c]	0.95
	1,2-dichloroethane	353[a]	311[a]	405[a]	0.01[a]	2.5[a]	0.04[a]	3.96		0.54		–	
	Water	354[d]	312[d]	423[d]	0.21[d]	9.2[d]	0.22[d]	0.86	53	0.44 (0.42 D_2O)	1.6	0.26[b]	0.96
Alloxazine (**2a**)[e]	Acetonitrile	372	320	432	0.009	0.35	0.26	28	10	0.36	2.8	2.42[b]	0.99
10-Et-5-deazaisoalloxazine (**3a**)[f]	Acetonitrile	397	317	467	0.16	4.05	0.40	2.1		0.25		2.42[b]	
5-Deazariboflavin (**3b**)[f]	Acetonitrile	399	329	457	0.11	4.03	0.27	2.2					
Lumiflavin (**4a**)[f]	Acetonitrile	443	342	533	0.16	7.7	0.21	1.1		0.41*		2.42[b]	
Riboflavin (**4b**)[f]	Acetonitrile	438		517	0.24	3.8	0.63	2.0					

λ_1, λ_2 are the positions of the two lowest-energy bands in the absorption spectra, λ_F the fluorescence emission maximum, Φ_F the fluorescence quantum yield, τ_F the fluorescence lifetime, k_r the radiative rate constant and Σk_{nr} the sum of nonradiative rate constants, τ_T the triplet lifetime, Φ_Δ the quantum yield of photosensitized production of singlet oxygen, τ_Δ singlet oxygen lifetimes ($\lambda_{exc}=371$ nm and $\lambda_{em}=1270$ nm), $k_T^{[O_2]}$ rate constant of quenching of triplet state by oxygen, [O_2] concentration of oxygen in a solvent at normal pressure, $P_T^\Delta = \frac{k_T^{[O_2]}\times[O_2]}{(\tau_T{}^{-1}+k_T^{[O_2]}\times[O_2])}$ is a proportion of triplet being quenched by molecular oxygen at normal pressure

*—note the new value 0.41, as estimated in the present work, which is in contrast to that we mistakenly reported before

[a]ref. [47]

[b]ref. [48]

[c]ref. [49]

[d]ref. [36]

[e]ref. [28]

[f]ref. [40] and references cited therein

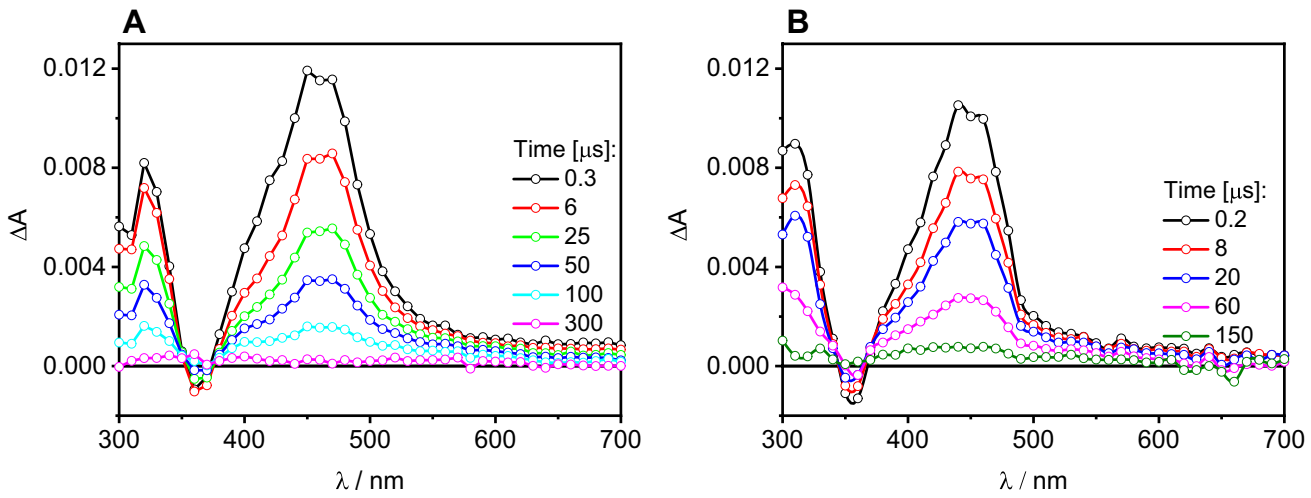

Fig. 3 Experimental transient absorption spectra of **1a** (**A**) in water (pH ~ 6) and (**B**) in acetonitrile, λ_{exc} = 355 nm, 0.5 mJ /pulse, argon-flushed solutions

of solvent acidity (hydrogen-bond donating ability) on the emission properties of **1a**. The absorption properties of **1a** in water and acetonitrile did not differ significantly; see Fig. 1S. However, the absorption spectrum in acetonitrile had more structure—there was a double maximum located near 300 nm (296 and 305 nm) in the short-wavelength part of the spectrum, and the long-wavelength maximum at 351 nm was flanked by two shoulders at 340 and 365 nm.

The solvent effect on the position of the emission maxima of **1a** is stronger than that on the absorption maxima of the respective compounds. The fluorescence spectrum of **1a** revealed slight differences in water vs. acetonitrile. The fluorescence maximum was located at 405 nm in acetonitrile, with a shoulder near 390 nm, while in water the fluorescence maximum was shifted towards the red, with a single peak at 423 nm. Thus, the Stokes shift was slightly higher in water (~ 4600 cm^{-1}) compared to acetonitrile (~ 3800 cm^{-1}). The fluorescence maxima in other solvents fell within the range delimited by those obtained in acetonitrile and water (Table 1). The fluorescence quantum yield had the highest values in methanol and water, while the lowest value was observed in 1,2-dichloroethane. The fluorescence lifetimes were all within the nanosecond timescale, from 2.5 ns in 1,2-dichloroethane to 9.2 ns in water. The fluorescence quantum yields indicate that excited state deactivation for **1a** proceeds mainly by non-radiative processes, such as internal conversion to the ground state and intersystem crossing to the triplet states, as well as chemical reactions. The increase of fluorescence of the **1a** in protic solvents can be explained by stabilization of the S_1 excited state by hydrogen bonding. This could simultaneously reduce the S_1 to T_1 radiationless intersystem crossing (ISC) rates. In water at pH 7.4 some of the contribution from the anion of isoalloxazine type of structure of **1a** can also be noticed [36], leading to stronger emission at longer wavelengths and larger Stokes shift in water comparing to **1a** in acetonitrile.

Assuming that Φ_Δ is expected to be smaller than or equal to the quantum yield of intersystem crossing Φ_{ISC} in the system under study, most of the deactivation is generally expected to go by intersystem conversion to populate the triplet state, as the singlet oxygen quantum yields indicate. In that context, it is interesting to consider $\Phi_F + \Phi_\Delta$, which for **1a** in acetonitrile is equal to 0.92 and in methanol is equal to 1, indicating that intersystem crossing to the triplet state and fluorescence are dominant processes in the relaxation of the singlet excited state. Lower values of $\Phi_F + \Phi_\Delta$ were obtained in dichloromethane and 1,2-dichloroethane, but this is largely due to the lower values of Φ_F (0.03 in dichloromethane and 0.01 in 1,2-dichloroethane), as the values of Φ_Δ remained relatively high (0.64 in dichloromethane and 0.54 in 1,2-dichloroethane). This points to a larger role of non-radiative internal conversion from the singlet excited state in dichloromethane and 1,2-dichloroethane. The magnitude of Φ_Δ is much lower (0.43) in water, but the Φ_F value of 0.21 indicates an important role for non-radiative channel $S_1 \rightarrow S_0$.

4.1 Transient absorption spectra of 1a in water (pH ~ 6) and acetonitrile

Compound **1a** upon laser excitation at 355 nm produced transient species in water (pH ~ 6) and in acetonitrile, decaying on the microsecond timescale, as shown in Fig. 3. The experimental transient absorption spectra of **1a** showed negative absorbance changes appearing around 360 nm as a result of the ground-state depletion, independent of the

solvent. At the same time, positive absorbance changes appeared around 320 and 450 nm. According to previous results drawn from the acid–base equilibria of **1a** at different pH, the neutral form of **1a** was present exclusively at pH ~ 6, without any other ionic or tautomeric forms, both in the ground and in the singlet excited state [36].

Global analysis of the transient absorption data for **1a** in the 300—700 nm spectral range showed the presence of characteristic time-components with decay times of 4.2 µs and 68 µs in water at pH ~ 6, and 12 µs and 59 µs in acetonitrile. The decay-associated spectra are shown in Fig. 2S; Fig. 3S additionally shows the transient absorption kinetics of **1a** at λ = 460 nm in the same solvent systems. The transient decay was well described by a bi-exponential function in both solvents, with time constants of 4.2 µs and 53.4 µs in water at pH ~ 6, and 12.5 µs and 60.8 µs in acetonitrile. It is proposed that the longer lifetime belongs to the triplet excited **1a** in all of the solvents used, whereas the shorter lifetime is attributed to triplet–triplet annihilation. An experiment with different laser energies was used to explore this hypothesis. An increase in the laser pulse energy resulted in the relative amplitude enhancement of the shorter-lived component, with no effect on the longer-lived component. Thus, Fig. 3 shows the results obtained for a lower laser pulse energy of 0.5 mJ, in order to reduce T-T annihilation while still maintaining a sufficiently high signal-to-noise ratio.

Steady-state absorption spectra were recorded for fresh and photolyzed solutions to verify the stability of **1a** in water (pH ~ 6) and acetonitrile solutions upon laser excitation (spectra not shown). No changes were noted in the UV–Vis absorption spectra before and after laser flash photolysis experiments, indicating that **1a** was quite stable under the experimental conditions, with no novel persistent photoproducts formed.

4.2 Quantum yield of intersystem crossing (Φ_{ISC}) for 1a in aqueous solutions

The quantum yield of intersystem crossing (Φ_{ISC}) for **1a** in aqueous solutions can be determined in two types of experiments: (1) transfer of the energy of the T_1 state to a reference dye acting as acceptor and (2) comparative actinometric measurements [50].

The spectral properties of **1a** and indicaxanthin (**5**) in water, and the excitation wavelength used (355 nm), were perfectly suited to the donor-**1a**-acceptor-**5** paradigm (see Fig. 4S). As a result of irradiation at 355 nm, an exclusive excitation of **1a** was achieved. Figure 4 shows transient absorption spectra of a mixture of **1a** and **5** in water (pH ~ 6). **5** is known to produce no triplet excited state

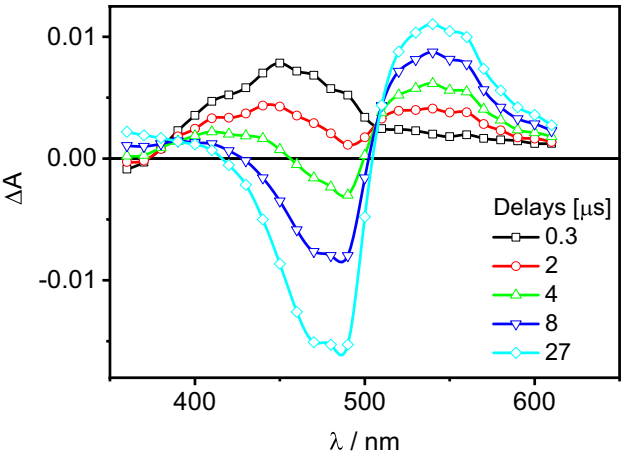

Fig. 4 Transient absorption spectra of the **1a** and **5** mixture in water (pH ~ 6); λ_{exc} = 355 nm, 0.5 mJ / pulse, argon-flushed solution at different time delays indicated in Figure. At initial delay 0.3 µs **1a** in the triplet excited state is observed at 450 nm by $T_1 \rightarrow T_n$ absorption band. At final time at 27 µs, a positive band of **5** in the triplet excited state is observed at 530 nm, as well as the **5** ground state bleaching at about 470 nm. This supports the mechanism of energy transfer from **1a** to **5**

through ISC ($S_1 \rightarrow T_1$) upon direct laser excitation at 355 nm [33]. However, when energy transfer was possible between **1a** and **5**, the value of the molar absorption coefficient of **1a** in its triplet excited state was determined ($\varepsilon_{T,5DAll}$ = 12.900 M^{-1} cm^{-1} at λ = 460 nm), using the extinction coefficient of **5** $\varepsilon_{T,IND}$ = 28.000 M^{-1} cm^{-1} at λ = 530 nm in water as a reference [33]. Note that the ε_T value of **1a** is quite close that of the alloxazine derivatives [8].

Next, the quantum yield value of the intersystem crossing quantum yield (Φ_{ISC}) of **1a** was determined in water, using a solution of benzophenone (**6**) in acetonitrile as a reference, based on Eq. (3):

$$\Phi_{ISC} = \Phi_{ISC}^{R} \times \frac{\varepsilon_T^R}{\varepsilon_T} \times \frac{\Delta A}{\Delta A^R} \quad (3)$$

Here, Φ_{ISC} is the quantum yield of intersystem crossing of **1a** in water, Φ_{ISC}^{R} is the same for **6** in acetonitrile, used as a reference with Φ_{ISC}^{R} = 1, [50] ε_T^R is the molar absorption coefficient of **6** in acetonitrile (reference; ε_T^R = 6500 M^{-1} cm^{-1} at λ = 520 nm) [50], ε_T is the same for **1a** in water (ε_T = 12.900 M^{-1} cm^{-1}), ΔA is the absorbance change of **1a** at λ = 460 nm (ΔA = 0.0101), ΔA^R is the same for the reference **6** in acetonitrile at λ = 520 nm (ΔA^R = 0.0120).

According to Eq. (3), the quantum yield of intersystem crossing of **1a** in water (pH ~ 6) was obtained: Φ_{ISC} = 0.43. This value agreed quite well with the quantum yield of singlet oxygen production for **1a** in both water and deuterated water (see the discussion below).

4.3 Deactivation of the singlet excited state of 1a in water

Earlier spectral and photophysical properties of **1a** and its 1,3-dimethyl derivative have been explored as a function of pH using different steady-state and time-resolved spectroscopic methods [32, 36], having found that **1a** existed in its neutral form at pH ~ 6. This neutral form had its fluorescence quantum yield $\Phi_F = 0.21$ and fluorescence lifetime $\tau_F = 9.2$ ns in aqueous solutions. Taking into account currently obtained value of $\Phi_{ISC} = 0.43$ and using the following definitions:

$$k_r = \Phi_F/\tau_F;$$

$$\sum k_{nr} = \left(1 - \Phi_F\right)/\boldsymbol{\tau}_F;$$

$$k_{IC} = \left[1 - \left(\Phi_F + \Phi_{ISC}\right)\right]/\tau_F;$$

$$k_{ISC} = \Phi_{ISC}/\tau_F;$$

the following values were calculated: radiative rate constant $k_r = 2.2 \times 10^7\ s^{-1}$; sum of non-radiative rate constants $\sum k_{nr} = 8.6 \times 10^7\ s^{-1}$; internal conversion rate constant $k_{IC} = 3.8 \times 10^7\ s^{-1}$ and intersystem crossing rate constant $k_{ISC} = 4.6 \times 10^7\ s^{-1}$.

It was therefore concluded that non-radiative processes were dominant in the deactivation of the singlet excited states for **1a**, as typically happens in organic solvents. When comparing non-radiative processes, the contribution of intersystem crossing ($S_1 \rightarrow T_1$) was slightly higher than that of internal conversion ($S_1 \rightarrow S_0$).

4.4 Singlet oxygen measurements

Isoalloxazine, deazaisoalloxazine, and alloxazine derivatives are interesting photosensitizers of singlet oxygen. However, there was a lack of information on singlet oxygen production by 5-deazaalloxazine **1a** and its derivatives. Therefore, photosensitization of singlet oxygen by **1a** was explored in organic solvents, including acetonitrile, methanol, dichloromethane, as well as in water and deuterated water. Note that due to the low $^1O_2$ intensity of 1270 nm emission, it was decided to conduct measurements in deuterated water instead regular water, due to the much longer lifetime of singlet oxygen in the latter (69 µs in D_2O *vs* 4.6 µs in H_2O). In these experiments, singlet oxygen emission was detected at 1270 nm, which is highly specific to the transition from the singlet excited state to the triplet ground state.

$$O_2\left(^1\Delta_g\right) \rightarrow O_2\left(^3\sum\nolimits_g^-\right) + h\nu$$

Measurements were performed in air-equilibrated solutions of **1a**, maintaining a constant oxygen concentration for a given solvent. It is well known that singlet oxygen may be produced by oxygen quenching of photosensitizer singlet or triplet excited states. When comparing the fluorescence lifetimes of **1a** in the nanosecond range with its triplet lifetimes in the microsecond range, it was concluded that **1a** should only generate singlet oxygen in solutions through its triplet state, as the probability of quenching of singlet state of **1a** should be very low due to its short fluorescence lifetime τ_F. Table 1 lists the values of the quantum yields of photosensitized production of singlet oxygen Φ_Δ by **1a** in selected organic solvents, as well as in water and deuterated water, with perinaphthenone (**7**) used as a reference. The values show that **1a** is a relatively efficient photosensitizer of singlet oxygen. Comparing data obtained in organic solvents, a higher value of Φ_Δ was obtained for **1a** in methanol ($\Phi_\Delta \sim 0.76$) compared to **1a** in acetonitrile ($\Phi_\Delta \sim 0.74$) and in dichloromethane ($\Phi_\Delta \sim 0.64$). A significantly lower value of Φ_Δ was observed in water and deuterated water ($\Phi_\Delta \sim 0.42$ and 0.44 respectively). Interestingly, these latter values were very close to $\Phi_{ISC} = 0.43$ of **1a** in water. Therefore, it is concluded that the proportion of triplet states quenched by oxygen was 0.96 in water. As a result, the quantum yield of the singlet oxygen for **1a** depended on the quantum yield of the formation of T_1. The reason for such a lower value of Φ_Δ (and ISC) in a case of **1a** is not clear. Some possibilities to explain the effect of water include proton transfer in the excited singlet state [47], or the energetic order of the $^1(n,\pi^*)$ and $^1(\pi,\pi^*)$ states [41], or modification of the ISC mechanism based on conical intersection [45].

Note that the concentration of oxygen might be the limiting factor in water, where it equals 0.26×10^{-3} M, while in acetonitrile and methanol it is approximately ten times higher [48]. Thus, apparently all excited triplets were transformed into singlet oxygen; see Table 1. The mechanism of energy transfer from the **1a** triplet state to oxygen was also confirmed, as the value of $k_T^{[O_2]}/k_{dyf}$ quite close to one-ninth [51], where, $k_T^{[O_2]}$ rate constant of quenching of triplet state by oxygen, k_{dyf} rate constants for reaction limited by diffusion.

For comparison, the value $\Phi_\Delta = 0.36$ for **2a** in acetonitrile [8] was lower than that for **1a** ($\Phi_\Delta \sim 0.70$, this work). Interestingly, lower Φ_Δ values were also observed in deuterated water compared to organic solvents for monomethyl alloxazine derivatives. Indeed, the Φ_Δ values for 9-methylalloxazine were 0.74 in acetonitrile, 0.88 in 1,2-dichloroethane, and 0.39 in deuterated water [22].

Table 1 lists also the lifetimes of singlet oxygen generated by **1a** in selected organic solvents, as well as in water and deuterated water. The decays recorded with $\lambda_{exc} = 371$ nm and $\lambda_{em} = 1270$ nm were all described by a mono-exponential function. The measured lifetimes were typical for singlet

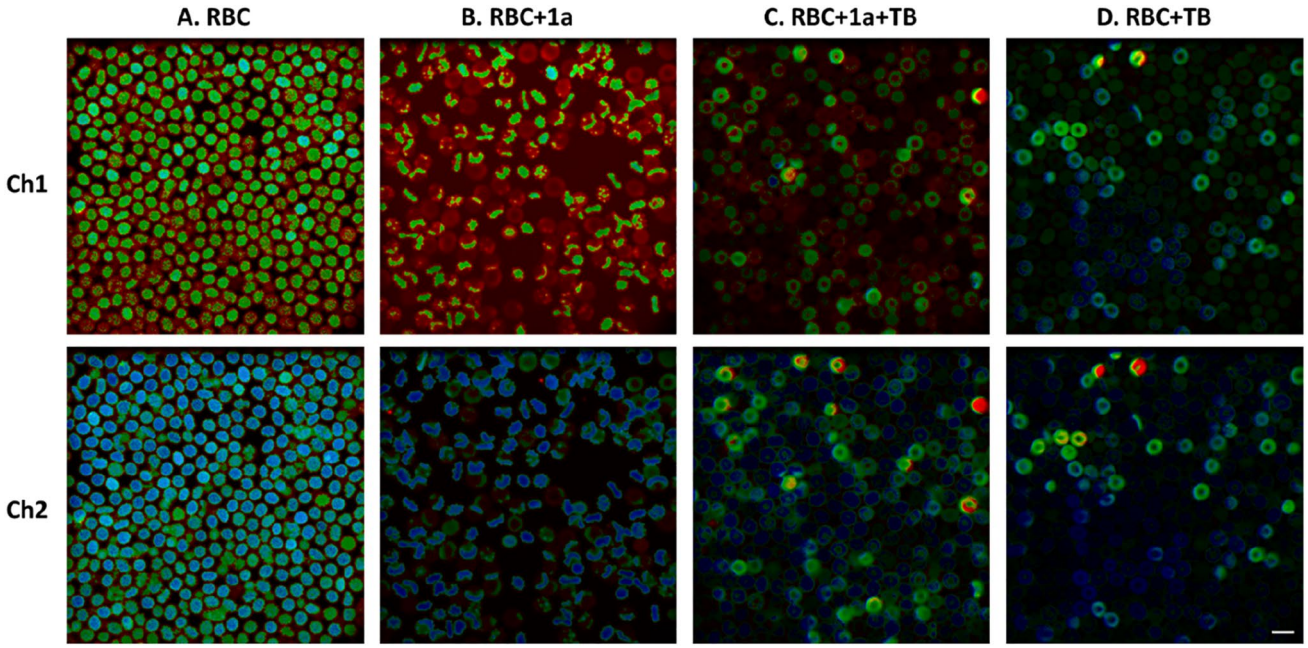

Fig. 5 Images of red blood cells (RBC) as obtained by FLIM (λ_{exc} = 405 nm emission recorded at two channels; channel 1: 420—550 nm and channel 2: 550—780 nm). RBC incubation condition: **A** control, in PBS buffer (24 h, 37 °C), **B** 1.0 mg/mL **1a** in PBS (24 h, 37° C), **C** 1.0 mg/mL **1a** (24 h, 37 °C) followed by incubation with 250 µM TB (1.5 h, at 37 °C), **D** in PBS buffer (24 h, 37 °C) followed by incubation with 250 µM TB (1.5 h, at 37 °C). Representative results are presented. Scale bar 10 µm

oxygen in the solvents used (4.6 µs in H_2O, 69 µs in D_2O, 11 µs in methanol, and 88 µs in dichloromethane) and are in agreement with the literature reports [51].

Additional measurements were taken to verify the stability of **1a** during the time-resolved measurements. Figures 5S and 6S show spectra and singlet oxygen decays generated by **1a** and **7** in acetonitrile, with λ_{exc} = 371 nm and λ_{em} = 1270 nm. Note that the absorbance values at the excitation wavelength remained unchanged during the experimental series for the **1a** and **7** solutions. Singlet oxygen emission decays were recorded during 300 s, with the singlet oxygen lifetimes remaining independent of the pre-irradiation time and always equal to 81 µs. Furthermore, singlet oxygen decays were measured at different absorbance values at λ_{exc} = 371 nm, ranging from 0.1 to 1.2, with six different samples of **1a** in each solvent. Once again, the measured singlet oxygen lifetimes were independent of the **1a** concentration, with standard characteristic decay times obtained in each of the solvents used. It was concluded that the SpectraLED diode did not produce any noticeable photodegradation, and that no novel photoproducts were generated. It was also concluded that **1a** was a good photosensitizer of singlet oxygen in a broad range of concentrations, independently of the solvent used, and singlet oxygen was never quenched by ground-state **1a**. Therefore, **1a** would be a convenient $^1O_2$ photosensitizer for studies that require singlet oxygen.

4.5 Hemolytic activity of 1a

In vitro evaluation of hemolytic activity is required before a compound may be deemed biocompatible [29]. The hemolytic activity of **1a** was analyzed at a concentration equal to 1.0 mg/mL in standard short-term incubation (1 h at 37 °C) and long-term incubation (24 h at 37 °C). After short-term (1 h) incubation, the degree of hemolysis of control RBC (incubated in PBS buffer) was equal to 2.5 ± 1.0%, *vs.* 2.8 ± 1.3% obtained for RBC incubated with **1a** (1.0 mg/mL). After long-term incubation (24 h), the degree of hemolysis was equal to 3.8 ± 1.6% for control RBC and 4.1 ± 1.7% for RBC incubated with **1a** (1.0 mg/mL), respectively. It should be noted that hemolysis values below 5% are assumed to indicate no hemolytic activity (no cell membrane-perturbing activity) of compound studied. Therefore, it can be concluded that **1a** at the concentration used (1.0 mg/mL) had no detrimental effects on the molecular structure of the lipid bilayer of the RBC membrane and is a suitable candidate for further evaluation in the cell system.

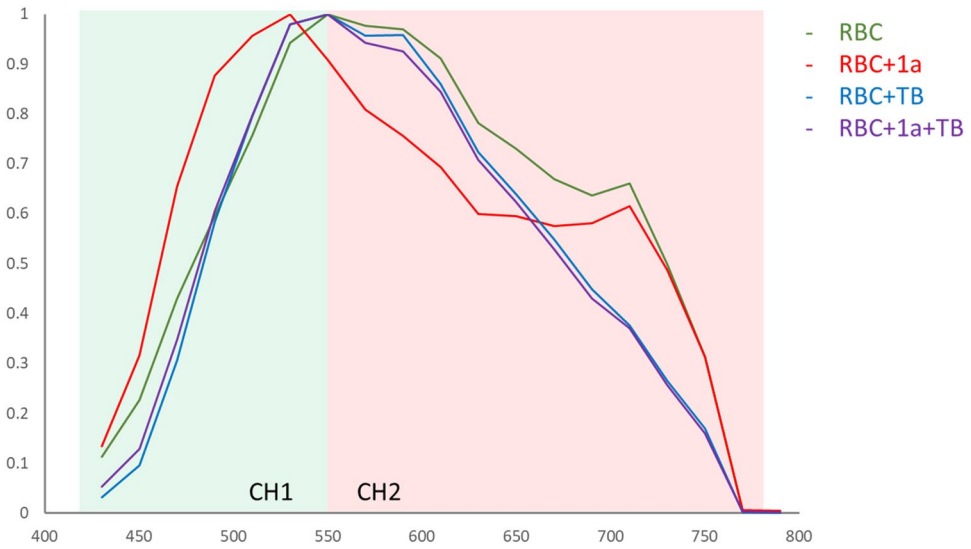

Fig. 6 Fluorescent emission spectra in cells. Excitation was at 405 nm, emission spectra were acquired without gating in the range from 420 to 800 nm with step of 20 nm on the same instrument with the same settings as FLIM acquisitions, except emission windows. RBC incubation condition (as in Fig. 5): green—control, in PBS buffer (24 h, 37 °C), red—1.0 mg/mL **1a** in PBS (24 h, 37° C), violet—1.0 mg/mL **1a** (24 h, 37 °C) followed by incubation with 250 µM TB (1.5 h, at 37 °C), blue—in PBS buffer (24 h, 37 °C) followed by incubation with 250 µM TB (1.5 h, at 37 °C). Representative results are presented

Table 2 Average lifetime distribution values of RBC, RBC treated with **1a**, RBC treated with **1a** and TB, RBC treated with TB for two spectral detection channels (3 fields of view per condition, > 100 cells per each field of view) of RBC

Parameter	A_1		A_2		τ_1		τ_2	
	Mean, kCnts	SEM, kCnts	Mean, kCnts	SEM, kCnts	Mean, ns	SEM, ns	Mean, ns	SEM, ns
RBC	4355	45	65	4	0.478	0.001	2.64	0.05
RBC + 1a	2353	188	317	6	0.495	0.003	5.72	0.07
RBC + TB	9091	170	159	7	0.517	0.002	4.10	0.00
RBC + 1a + TB	11,355	252	340	12	0.527	0.002	4.18	0.08
RBC	8459	133	332	8	0.431	0.002	1.84	0.06
RBC + 1a	5212	370	188	2	0.437	0.001	3.98	0.08
RBC + TB	16,222	318	313	16	0.531	0.001	3.03	0.03
RBC + 1a + TB	24,304	644	552	16	0.545	0.004	3.16	0.04

$\mathbf{A_1}$ and $\mathbf{A_2}$ are the amplitudes of the dual exponential fit that represent the number of photon counts (in thousands of counts). τ_1 and τ_2 are corresponding decay times (in ns), SEM is standard error of mean. Top half of the table (rows 1–4) corresponds to the data acquired by emission channel 1 (420–550 nm), lower half (rows 5–8 – channel 2 (550–780 nm)

4.6 Fluorescence lifetime distribution in RBC under physiological and oxidative stress conditions

In search of potential biological applications, **1a** was studied in human RBC under physiological-like and oxidative stress conditions. Specifically, FLIM (Fluorescence Lifetime Imaging Microscopy) experiments were performed on **RBC** after excitation at 405 nm and emission was recorded in two channels (channel 1: 420—550 nm and channel 2: 550—780 nm), enabling finer monitoring of changes in fluorescent properties in cells by separating the emissions from potentially different species. As shown in Fig. 5, **RBC** treated with **1a** at physiological-like conditions (5B – **RBC + 1a**) are different from untreated cells (5A—**RBC**). Exposing **RBC** to oxidative stress by incubation with *tert*-butyl hydroperoxide further changes the status of RBC, as shown in FLIM images (5C – **RBC + 1a + TB** and 5D – **RBC + TB**).

It should be noted that the differences are more pronounced in channel 1, which can theoretically record the emission of both endogenous species (such as nicotinamide and flavin derivatives) and **1a** itself. The wider emission band in channel 1 of the spectrum collected in cells treated

Table 3 Decay times comparison for first ten vs last ten frames collected for representative fields of view for each condition

Parameter	A_1		A_2		τ_1		τ_2	
Frames	1–10	91–100	1–10	91–100	1–10	91–100	1–10	91–100
RBC	266	615	9	4.7	0.49	0.47	2.23	3.20
RBC + 1a	120	2057	28	315	0.49	0.50	5.30	5.64
RBC + TB	857	912	20	12	0.53	0.51	4.12	4.20
RBC + 1a + TB	1131	1063	40	27	0.55	0.51	4.20	4.45
RBC	318	1277	34	30	0.46	0.43	2.02	1.88
RBC + 1a	204	4653	17	181	0.46	0.44	3.70	3.92
RBC + TB	1533	1578	34	26	0.57	0.51	3.33	2.90
RBC + 1a + TB	2468	2076	62	45	0.59	0.51	3.48	3.01

A_1 and **A_2** are the amplitudes of the dual exponential fit that represent the number of photon counts (in thousands of counts). τ_1 and τ_2 are corresponding decay times (in ns), Top half of the table (rows 1–4) corresponds to the data acquired by emission channel 1 (420–550 nm), lower half (rows 5–8) – channel 2 (550–780 nm). Frames 1–10 show combined fit values for the first 10 frames of the acquisition, when 91–100 – values for last 10 acquired frames

with **1a** (**RBC + 1a**) vs untreated **RBC** further suggests a potential contribution of **1a** to the fluorescence in channel 1 (Fig. 6 red vs green). Channel 2, in turn, covers principally autofluorescence of the cells. These same data also indicate that oxidatively stressed cells, exposed to *tert*-butyl hydroperoxide (**TB**), exhibit the same emission spectrum independently of whether they were treated with **1a** or not, suggesting that in the case of **TB** samples, **1a** does not substantially contribute to fluorescence emission (Fig. 6 blue and violet).

The differences discussed above were further confirmed by a more detailed analysis of the deconvoluted lifetime distribution (Fig. 7S) and the average values of the fluorescence lifetime parameters (Table 2), all calculated using original FLIM experiments (three images per condition composed of 100 consecutively recorded frames, each image containing more than 100 single cells) by a double-exponential fit after subtraction of the instrument response function.

Lower amplitudes (Table 2) for **RBC + 1a** vs untreated **RBC** at physiological-like conditions point at decreasing fluorescence emission intensity in the presence of **1a.** It is also accompanied by a lengthening and increase in the amplitude of the longer lifetime component τ_2 in channel 1 (rows 1–4 in Table 2: $\tau_{2\ \mathbf{RBC+1a}} = 5.72$ ns (12%) vs **RBC** $\tau_{2\ \mathbf{RBC}} = 2.64$ ns (1.5%)) with a shorter component remaining similar (approx. 0.49 ns). Interestingly, oxidative stress (pre-incubation of cells with TB) leads to a similar value of longer lifetime component τ_2 for both **RBC + TB** and **RBC + 1a + TB**, placing it in between **RBC + 1a** and **RBC**, in a decreasing order: $\tau_{2\ \mathbf{RBC+1a}} = 5.72$ ns $> \tau_{2\ \mathbf{RBC+1a+TB}} = 4.18$ ns $> \tau_{2\ \mathbf{RBC+TB}} = 4.10$ ns $> \tau_{2\ \mathbf{RBC}} = 2.64$ ns. On the other hand, there was only a small difference in the value of the short components between the **RBC** treated with or without **1a**. In channel 2 (rows 5–8 in Table 2) the longer lifetime components were similarly generally shorter than the analogous parameters in channel 1 but the order was similar and followed the trend $\tau_{2\ \mathbf{RBC+1a}} = 3.98$ ns $> \tau_{2\ \mathbf{RBC+1a+TB}} = 3.16$ ns $> \tau_{2\ \mathbf{RBC+TB}} = 3.03$ ns $> \tau_{2\ \mathbf{RBC}} = 1.84$ ns. Interestingly, for channel 2, a shorter component seemed to be independent on the oxidative state of the cells, following the order $\tau_{1\ \mathbf{RBC+1a}} = 0.43$ ns $= \tau_{1\ \mathbf{RBC+1a+TB}} = 0.43$ ns $< \tau_{1\ \mathbf{RBC+TB}} = 0.53$ ns $= \tau_{1\ \mathbf{RBC}} = 0.54$ ns.

Importantly, treatment of cells with **TB** clearly leads to an increase in the fluorescence intensity, with a larger effect being observed for the cells incubated with **1a** (amplitudes in Table 2). In addition, by comparing the FLIM data of the first and last 10 frames of 100 frames series collected for each field of view, it was shown, that the intensity of the fluorescence increases in time of the exposure of the cells to the excitation laser, but this increase is substantially more pronounced for the cells treated with **1a** (Table 3). This observation suggests a light-dependent influence of the **1a** on the oxidative environment of the cells, in line with its capacity of singlet-oxygen generation. At the same time, fluorescent lifetimes calculated separately for first vs last 10 frames show only modest change proving a better robustness of this parameter in monitoring oxidative state of the cells.

5 Conclusions

On the basis of obtained results, we can state that photolysis of **1a** leads to generation of the triplet excited states in high yields both in organic solvents and in water. The **1a** triplet lifetime, independently of the solvent, was always on the tens of microsecond time range. Thus, the photophysical behavior of this compound was quite similar to that of **2a** and its derivatives.

The characteristic singlet oxygen emission generated by **1a** in selected organic solvents and in deuterated water in the NIR spectral range ($\lambda_{em} \sim 1270$ nm) was recorded using

steady-state and time-resolved techniques, showing **1a** to be an efficient singlet oxygen photosensitizer. Due to the short fluorescence lifetimes of **1a**, its singlet excited state practically did not contribute to singlet oxygen generation.

The Φ_Δ values in deuterated water were lower than those in organic solvents. The intersystem crossing quantum yield $\Phi_{ISC} = 0.43$ was obtained for **1a** in water, based on experiments involving triplet energy transfer and comparative actinometric measurements. The proposed method of determining Φ_{ISC} based on the usage of indicaxanthin (**5**) appeared to be quite useful and could be used to extract Φ_{ISC} values for a range of alloxazine derivatives in aqueous solutions. Very similar values of singlet oxygen yield generated by **1a** ($\Phi_\Delta = 0.42$ and 0.44) were obtained in water and deuterated water, respectively. As far as oxygen quenching of triplet states is concerned, the rate constants for the process are on the order of magnitude 1.2×10^9 M^{-1} s^{-1} or higher, therefore, for the triplet state lifetimes exceeding 10 µs most of the triplet states are quenched by oxygen in air saturated solutions, with the respective fraction exceeding 95%.

The detection of characteristic spectra with a maximum at 1270 nm and their emission kinetics directly confirm the existence of singlet oxygen in the case of excitation of **1a** in water. The formed triplet was almost entirely quenched, $P_T^\Delta = 0.96$, by the molecular oxygen dissolved in water at normal pressure. The intersystem crossing quantum yield of **1a** in water was measured as $\Phi_{ISC} = 0.43$, and the quantum yield of the photosensitized production of singlet oxygen was $\Phi_\Delta = 0.44$, which values are nearly identical. Additionally, in laser flash photolysis experiment, no transient signals from radicals could be detected, while the fluorescence quantum yield was $\Phi_F = 0.21$.

Regarding the potential biological applications of **1a** and similar compounds, the FLIM data were interpreted using the lifetime distribution analysis and comparing the properties of human RBC under oxidative stress conditions in the presence and absence of **1a**. Based on the preliminary study using RBC, it was concluded that **1a** is a biocompatible, non-hemolytic compound at concentration equal to 1.0 mg/mL in both short-term (1 h) and long-term (24 h) incubation. Differences in fluorescence lifetime parameters obtained from FLIM experiments for pre-incubated RBC with **1a** can be used for monitoring the oxidative state of the cells. In addition, analysis of FLIM data from different channels (different emission wavelengths) can provide complementary information to shed light on deciphering the relationship between the cell-derived and probe-driven impact on the cellular environment.

Supplementary Information The online version contains supplementary material available at https://doi.org/10.1007/s43630-023-00401-9.

Acknowledgements This paper is dedicated to the memory of David R. Worrall. This study was supported by the research grants 2017/27/B/ST4/02494 (OPUS) and NCN CEUS-UNISONO 2020/02/Y/ST4/00042, both from The National Science Centre of Poland (NCN) and by grant 21-14200K from the Czech Science Foundation. MG would like to express his thanks to The National Science Centre of Poland (NCN) for financial support from grant 2013/08/T/ST4/00640 (Etiuda). JLK would like to acknowledge the financial support of the grant no POIR.04.04.00-00-441F/17-00 within HOMING programme of the Foundation for Polish Science co-financed by the European Union under the European Regional Development Fund and financial support from the grant 2018/29/B/ST4/01498 (Opus) for the National Science Centre of Poland (NCN). JLK, DK and VCh would like to acknowledge the financial support of the POIR.04.02.00-00-C004/19-00 project funded under the Smart Growth Operational Programme 2014-2020, co-financed by the European Union through the European Regional Development Fund and financial support from the Polish Ministry of Education and Science (previously MNiSW, decision no DIR/WK/2018/06) for involvement in the joint international project entitled European Infrastructure of Open Screening Platforms of Chemical Biology European Research Infrastructure Consortium (EU-OPENSCREEN ERIC). We are grateful Dr. S. Wybraniec for providing purified indicaxanthin used in actinometric measurements.

Author contributions The following co-authors contributed in particular with; MI-R and AG: steady state and time resolved experiments with 1a in different solvents. AG: singlet oxygen measurements, JLK, VCh, DK- FLIM experiments, its analysis and figures related to FLIM, MG steady state and time resolved experiments with 1a GB: laser flash photolysis experiments and its analysis, interpretation and respective figures preparation. ZA: singlet oxygen measurements. ES: conceptualization, methodology, formal analysis, A-TEEMs™ experiments. IK: conceptualization. RC, JLM, LM and MS: supervision, funding acquisition, conceptualization, methodology, formal analysis, investigation, writing original draft. Four lead scientists RC, JLK, LM, and MS supervised respective areas of research: RC – organic chemistry, JLK – FLIM, LM – biochemistry, MS – photochemistry and total coverage of the project. All authors reviewed the manuscript.

Data availability The datasets generated during the current study are available from the corresponding author on reasonable request.

Declarations

Conflict of interest The authors declare that they have no known competing financial interests or personal relationships that could have appeared to influence the work reported in this paper.

References

1. Yeow, J., Kaur, A., Anscomb, M. D., & New, E. J. (2014). A novel flavin derivative reveals the impact of glucose on oxidative stress in adipocytes. *Chemical Communications (Cambridge, England), 50*, 8181–8184. https://doi.org/10.1039/c4cc03464c

2. Kaur, A., Haghighatbin, M. A., Hogan, C. F., & New, E. J. (2015). A FRET-based ratiometric redox probe for detecting oxidative stress by confocal microscopy, FLIM and flow cytometry. *Chemical Communications (Cambridge, England), 51*, 10510–10513. https://doi.org/10.1039/c5cc03394b
3. Kolanowski, J. L., Kaur, A., & New, E. J. (2016). Selective and reversible approaches toward imaging redox signaling using small-molecule probes. *Antioxidants and Redox Signaling, 24*, 713–730. https://doi.org/10.1089/ars.2015.6588
4. Hong, K. I., Lee, S. M., & Jang, W. D. (2018). Flavin-based light-driven fluorescent probe for the detection of antioxidant amino acids. *ChemistryOpen, 7*, 57–60. https://doi.org/10.1002/open.201700144
5. Mojr, V., Pitrova, G., Strakova, K., Prukała, D., Brazevic, S., Svobodova, E., Hoskovcova, I., Burdziński, G., Slanina, T., Sikorski, M., & Cibulka, R. (2018). Flavin photocatalysts for visible-light 2+2 cycloadditions: Structure, reactivity and reaction mechanism. *ChemCatChem, 10*, 849–858. https://doi.org/10.1002/cctc.201701490
6. Graml, A., Nevesely, T., Jan Kutta, R., Cibulka, R., & König, B. (2020). Deazaflavin reductive photocatalysis involves excited semiquinone radicals. *Nature Communications, 11*, 3174. https://doi.org/10.1038/s41467-020-16909-y
7. Cardoso, D. R., Libardi, S. H., & Skibsted, L. H. (2012). Riboflavin as a photosensitizer. Effects on human health and food quality. *Food & Function, 3*, 487–502. https://doi.org/10.1039/c2fo10246c
8. Sikorska, E., Sikorski, M., Steer, R. P., Wilkinson, F., & Worrall, D. R. (1998). Efficiency of singlet oxygen generation by alloxazines and isoalloxazines. *Journal of the Chemical Society, Faraday Transactions, 94*, 2347–2353. https://doi.org/10.1039/a802340i
9. Sikorska, E., Khmelinskii, I., Komasa, A., Koput, J., Ferreira, L. F. V., Herance, J. R., Bourdelande, J. L., Williams, S. L., Worrall, D. R., Insińska-Rak, M., & Sikorski, M. (2005). Spectroscopy and photophysics of flavin related compounds: Riboflavin and iso-(6,7)-riboflavin. *Chemical Physics, 314*, 239–247. https://doi.org/10.1016/j.chemphys.2005.03.005
10. Baier, J., Maisch, T., Maier, M., Engel, E., Landthaler, M., & Baumler, W. (2006). Singlet oxygen generation by UVA light exposure of endogenous photosensitizers. *Biophysical Journal, 91*, 1452–1459. https://doi.org/10.1529/biophysj.106.082388
11. Engl, R., Kilger, R., Maier, M., Scherer, K., Abels, C., & Baumler, W. (2002). Singlet oxygen generation by 8-methoxypsoralen in deuterium oxide: Relaxation rate constants and dependence of the generation efficacy on the oxygen partial pressure. *The Journal of Physical Chemistry B, 106*, 5776–5781. https://doi.org/10.1021/jp013727y
12. Vakrat-Haglili, Y., Weiner, L., Brumfeld, V., Brandis, A., Salomon, Y., McIlroy, B., Wilson, B. C., Pawlak, A., Rozanowska, M., Sarna, T., & Scherz, A. (2005). The microenvironment effect on the generation of reactive oxygen species by Pd-bacteriopheophorbide. *Journal of the American Chemical Society, 127*, 6487–6497. https://doi.org/10.1021/ja046210j
13. Tanielian, C., Schweitzer, C., Mechin, R., & Wolff, C. (2001). Quantum yield of singlet oxygen production by monomeric and aggregated forms of hematoporphyrin derivative. *Free Radical Biology & Medicine, 30*, 208–212. https://doi.org/10.1016/s0891-5849(00)00460-3
14. Hanson, K. M., & Simon, J. D. (1998). Epidermal trans-urocanic acid and the UV-A-induced photoaging of the skin. *Proceedings of the National academy of Sciences of the United States of America, 95*, 10576–10578. https://doi.org/10.1073/pnas.95.18.10576
15. Lu, C. Y., Han, Z. H., Liu, G. S., Cai, X. C., Chen, Y. L., & Yao, S. (2001). Photophysical and photochemical processes of riboflavin (vitamin B-2) by means of the transient absorption spectra in aqueous solution. *Sci. China, B Chem., 44*, 39–48. https://doi.org/10.1007/bf02879734
16. Insińska-Rak, M., Sikorska, E., Bourdelande, J. L., Khmelinskii, I. V., Prukała, W., Dobek, K., Karolczak, J., Machado, I. F., Ferreira, L. F. V., Komasa, A., Worrall, D. R., & Sikorski, M. (2006). Spectroscopy and photophysics of flavin-related compounds: 5-deazariboflavin. *Journal of Molecular Structure, 783*, 184–190. https://doi.org/10.1016/j.molstruc.2005.09.005
17. Heelis, P. F. (1982). The photophysical and photochemical properties of flavins (isoalloxazines). *Chemical Society Reviews, 11*, 15–39. https://doi.org/10.1039/cs9821100015
18. Salzmann, S., Martinez-Junza, V., Zorn, B., Braslavsky, S. E., Mansurova, M., Marian, C. M., & Gärtner, W. (2009). Photophysical properties of structurally and electronically modified flavin derivatives determined by spectroscopy and theoretical calculations. *Journal of Physical Chemistry A, 113*, 9365–9375. https://doi.org/10.1021/jp905724b
19. Neiss, C., Saalfrank, P., Parac, M., & Grimme, S. (2003). Quantum chemical calculation of excited states of flavin-related molecules. *Journal of Physical Chemistry A, 107*, 140–147. https://doi.org/10.1021/jp021671h
20. Sikorski, M., Sikorska, E., Koziołowa, A., Moreno, R. G., Bourdelande, J. L., Steer, R. P., & Wilkinson, F. (2001). Photophysical properties of lumichromes in water. *Journal of Photochemistry and Photobiology A: Biology, 60*, 114–119. https://doi.org/10.1016/S1011-1344(01)00134-8
21. Sikorska, E., Khmelinskii, I. V., Prukała, W., Williams, S. L., Worrall, D. R., Bourdelande, J. L., Bednarek, A., Koput, J., & Sikorski, M. (2004). Spectroscopy and photophysics of 9-methylalloxazine. Experimental and theoretical study. *Journal of Molecular Structure, 689*, 121–126. https://doi.org/10.1016/j.molstruc.2003.10.28
22. Sikorska, E., Khmelinskii, I. V., Bourdelande, J. L., Bednarek, A., Williams, S. L., Patel, M., Worrall, D. R., Koput, J., & Sikorski, M. (2004). Spectroscopy and photophysics of mono methyl-substituted alloxazines. *Chemical Physics, 301*, 95–103. https://doi.org/10.1016/j.chemphys.2004.03.005
23. Grodowski, M. S., Veyret, B., & Weiss, K. (1977). Photochemistry of flavins.2. Photophysical properties of alloxazines and isoalloxaznies. *Photochemistry and Photobiology, 26*, 341–352. https://doi.org/10.1111/j.1751-1097.1977.tb07495.x
24. Encinas, M. V., Bertolotti, S. G., & Previtali, C. M. (2002). The interaction of ground and excited states of lumichrome with aliphatic and aromatic amines in methanol. *Helvetica Chimica Acta, 85*, 1427–1438. https://doi.org/10.1002/1522-2675(200205)85:5%3c1427::AID-HLCA1427%3e3.0.CO;2-A
25. Li, H., Jiang, Z. Q., Pan, Y., & Yu, S. Q. (2006). Study on electron transfer of fluorescent probe lumichrome and nucleic acid by laser flash photolysis. *Research on Chemical Intermediates, 32*, 695–708
26. Davis, C. A., Erickson, P. R., McNeill, K., & Janssen, E. M. L. (2017). Environmental photochemistry of fenamate NSAIDs and their radical intermediates. *Environmental Science. Processes & Impacts, 19*, 656–665. https://doi.org/10.1039/c7em00079k
27. Sikorska, E., Khmelinskii, I. V., Prukała, W., Williams, S. L., Patel, M., Worrall, D. R., Bourdelande, J. L., Koput, J., & Sikorski, M. (2004). Spectroscopy and photophysics of lumiflavins and lumichromes. *Journal of Physical Chemistry A, 108*, 1501–1508. https://doi.org/10.1021/jp037048u
28. Sikorski, M., Prukała, D., Insińska-Rak, M., Khmelinskii, I., Worrall, D. R., Williams, S. L., Hernando, J., Bourdelande, J. L., Koput, J., & Sikorska, E. (2008). Spectroscopy and photophysics of dimethyl-substituted alloxazines. *Journal of Photochemistry and Photobiology A: Chemistry, 200*, 148–160. https://doi.org/10.1016/j.jphotochem.2008.07.006
29. Greco, I., Molchanova, N., Holmedal, E., Jenssen, H., Hummel, B. D., Watts, J. L., Håkansson, J., Hansen, P. R., & Svenson, J. (2020). Correlation between hemolytic activity, cytotoxicity and

systemic in vivo toxicity of synthetic antimicrobial peptides. *Sci. Rep*. https://doi.org/10.1038/s41598-020-69995-9
30. Farag, M. R., & Alagawany, M. (2018). Erythrocytes as a biological model for screening of xenobiotics toxicity. *Chemico-Biological Interactions, 279*, 73–83. https://doi.org/10.1016/j.cbi.2017.11.007
31. Mohanty, J. G., Nagababu, E., & Rifkind, J. M. (2014). Red blood cell oxidative stress impairs oxygen delivery and induces red blood cell aging. *Frontiers in Physiology, 5*, 84. https://doi.org/10.3389/fphys.2014.00084
32. Prukała, D., Gierszewski, M., Pędziński, T., & Sikorski, M. (2014). Influence of pH on spectral and photophysical properties of 9-methyl-5-deazaalloxazine and 10-ethyl-5-deaza-isoalloxazine. *Journal of Photochemistry and Photobiology A: Chemistry, 275*, 12–20. https://doi.org/10.1016/j.jphotochem.2013.10.011
33. Wendel, M., Szot, D., Starzak, K., Tuwalska, D., Prukała, D., Pędziński, T., Sikorski, M., Wybraniec, S., & Burdziński, G. (2015). Photophysical properties of indicaxanthin in aqueous and alcoholic solutions. *Dyes and Pigments, 113*, 634–639. https://doi.org/10.1016/j.dyepig.2014.09.036
34. Taylor, E. C., Jr., & Kalenda, N. W. (1956). The synthesis of pyrimido[4,5-b]quinolines. *Journal of the American Chemical Society, 78*, 5108–5115. https://doi.org/10.1021/ja01600a079
35. Kokel, B. (1994). The reaction of N, N-dimethyldichloromethyleniminium chloride (phosgeniminium chloride) with 6-N-arylaminouracils. A new and convenient "one pot" synthesis of l,3-dimethyl-5- dimethylaminopyrimido[4,5-b]quinoline-(1H,3H)-2,4-diones, 1,3-dimethyl-5-chloropyrimido[4,5-b]quinoline-(1H,3H)-2,4-diones and 3-methyl-10-alkyl-5-chloropyrimido[4,5-b]quinoline-(3H,10H)-2,4-diones (3-methyl-10-alkyl-5-chloro-5-deazaflavins). *Journal of Heterocyclic Chemistry, 31*, 845–855. https://doi.org/10.1002/jhet.5570310427
36. Prukała, D., Gierszewski, M., Karolczak, J., & Sikorski, M. (2015). Study of photophysical properties of 5-deazaalloxazine and 1,3-dimethyl-5-deazaalloxazine in dependence of p*H* using different spectral techniques. *Physical Chemistry Chemical Physics: PCCP, 17*, 18729–18741. https://doi.org/10.1039/c5cp01566a
37. Burdziński, G., Maciejewski, A., Buntinx, G., Poizat, O., & Lefumeux, C. (2004). Ultrafast quenching of the excited S_2 state of benzopyranthione by acetonitrile. *Chemical Physics Letters, 384*, 332–338. https://doi.org/10.1016/j.cplett.2003.12.029
38. Schmidt, R., Tanielian, C., Dunsbach, R., & Wolff, C. (1994). Phenalenone, a universal reference compound for the determination of quantum yields of singlet oxygen $O_2(^1\Delta_g)$ sensitization. *Journal of Photochemistry and Photobiology A: Chemistry, 79*, 11–17. https://doi.org/10.1016/1010-6030(93)03746-4
39. Mrówczyńska, L., & Hägerstrand, H. (2009). Platelet-activating factor interaction with the human erythrocyte membrane. *Journal of Biochemical Toxicology, 23*, 345–348. https://doi.org/10.1002/jbt.20297
40. Sikorski, M., Khmelinskii, I., & Sikorska, E. (2021). Spectral Properties of Flavins. In R. Cibulka & M. Fraaije (Eds.), *Flavin-Based Catalysis* (pp. 67–96). Weinheim, Germany: Wiley-VCH.
41. Salzmann, S., & Marian, C. M. (2009). The photophysics of alloxazine: A quantum chemical investigation in vacuum and solution. *Photochemical & Photobiological Sciences, 8*, 1655–1666. https://doi.org/10.1039/b9pp00022d
42. Moyon, N. S., & Mitra, S. (2011). Fluorescence solvatochromism in lumichrome and excited-state tautomerization: a combined experimental and DFT study. *Journal of Physical Chemistry A, 115*, 2456–2464. https://doi.org/10.1021/jp1102687
43. Sikorska, E., Szymusiak, H., Khmelinskii, I. V., Koziołowa, A., Spanget-Larsen, J., & Sikorski, M. (2003). Spectroscopy and photophysics of alloxazines studied in their ground and first excited singlet states. *Journal of Photochemistry and Photobiology A: Chemistry, 158*, 45–53. https://doi.org/10.1016/s1010-6030(03)00104-7
44. Sikorska, E., Khmelinskii, I. V., Nowacka, G., Koput, J., & Sikorski, M. (2005). Spectroscopy and photophysics of cyanoalloxazines. Theoretical study. *Journal of Molecular Structure: THEOCHEM, 722*, 51–56. https://doi.org/10.1016/j.theochem.2004.11.058
45. Chang, X. P., Xie, X. Y., Lin, S. Y., & Cui, G. L. (2016). QM/MM Study on mechanistic photophysics of alloxazine chromophore in aqueous solution. *Journal of Physical Chemistry A, 120*, 6129–6136. https://doi.org/10.1021/acs.jpca.6b02669
46. Prukała, D., Taczkowska, M., Gierszewski, M., Pędziński, T., & Sikorski, M. (2014). Spectroscopy and photophysics of monomethyl-substituted derivatives of 5-deazaalloxazine and 10-ethyl-5-deaza-isoalloxazine. *Journal of Fluorescence, 24*, 505–521. https://doi.org/10.1007/s10895-013-1320-9
47. Prukała, D., Khmelinskii, I., Koput, J., Gierszewski, M., Pędziński, T., & Sikorski, M. (2014). Photophysics, excited-state double-proton transfer and hydrogen-bonding properties of 5-deazaalloxazines. *Photochemistry and Photobiology, 90*, 972–988. https://doi.org/10.1111/php.12289
48. Quaranta, M., Murkovic, M., & Klimant, I. (2013). A new method to measure oxygen solubility in organic solvents through optical oxygen sensing. *The Analyst, 138*, 6243–6245. https://doi.org/10.1039/c3an36782g
49. Sato, T., Hamada, Y., Sumikawa, M., Araki, S., & Yamamoto, H. (2014). Solubility of oxygen in organic solvents and calculation of the Hansen solubility parameters of oxygen. *Industrial and Engineering Chemistry Research, 53*, 19331–19337. https://doi.org/10.1021/ie502386t
50. Carmichael, I., & Hug, G. L. (1986). Triplet-triplet absorption-spectra of organic-molecules in condensed phases. *Journal of Physical and Chemical Reference Data, 15*, 1–250. https://doi.org/10.1063/1.555770
51. Wilkinson, F., Helman, W. P., & Ross, A. B. (1993). Quantum yields for the photosensitized formation of the lowest electronically excited singlet-state of molecular-oxygen in solution. *Journal of Physical and Chemical Reference Data, 22*, 113–262. https://doi.org/10.1063/1.555934

Authors and Affiliations

Małgorzata Insińska-Rak[1] · Anna Golczak[1] · Mateusz Gierszewski[2] · Zubair Anwar[1] · Volodymyr Cherkas[3] · Dorota Kwiatek[3] · Ewa Sikorska[4] · Igor Khmelinskii[5] · Gotard Burdziński[2] · Radek Cibulka[6] · Lucyna Mrówczyńska[7] · Jacek Lukasz Kolanowski[3] · Marek Sikorski[1]

✉ Radek Cibulka
cibulkar@vscht.cz

✉ Lucyna Mrówczyńska
lumro@amu.edu.pl

✉ Jacek Lukasz Kolanowski
jacek.kolanowski@ibch.poznan.pl

✉ Marek Sikorski
sikorski@amu.edu.pl

[1] Faculty of Chemistry, Adam Mickiewicz University, Uniwersytetu Poznańskiego 8, 61-614 Poznań, Poland

[2] Faculty of Physics, Adam Mickiewicz University, Uniwersytetu Poznańskiego 2, 61-614 Poznań, Poland

[3] Institute of Bioorganic Chemistry, Polish Academy of Sciences, Noskowskiego 12-14, 61-704 Poznań, Poland

[4] Poznań University of Economics and Business, Al. Niepodległości 10, 61-875 Poznań, Poland

[5] Department of Chemistry and Pharmacy, Faculty of Sciences and Technology, and Centre for Electronics, Optoelectronics and Telecommunications, University of the Algarve, 8005-139 Faro, Portugal

[6] Department of Organic Chemistry, University of Chemistry and Technology, Prague, Technicka 5, Prague 6, 16628 Prague, Czech Republic

[7] Faculty of Biology, Adam Mickiewicz University, Uniwersytetu Poznańskiego 6, 61-614 Poznań, Poland